HIGH VELOCITY IMPACT RESPONSE OF HYBRID PSEUDO-WOVEN FIBER-REINFORCED COMPOSITE LAMINATES

Cyrus Vakili Rad [a,b], Julie Roark [a,b], Duane Revilock [c], Ramy Harik [a,b], Subramani Sockalingam[a,b] , Zafer Gurdal [a,b],

[a] McNair Center for Aerospace Innovation and Research, University of South Carolina, SC, USA
[b] Department of Mechanical Engineering, University of South Carolina, SC, USA
[c] Impact Dynamics Group, NASA Glenn Research Center, OH, USA

ABSTRACT

An intermediary architecture of woven laminates and unidirectional laminates, referred to as pseudo-woven laminates, is proposed as an alternative hybridized structure to improve impact properties of composite laminates. Pseudo-woven laminates make use of an automated fiber placement (AFP) manufacturing process to produce a unique laminate architecture. These laminates are heterogeneous with spatially defined features where elasticity tensor is spatially variable unlike traditional composites. The heterogeneity is associated with interply locking and topological variations in the fiber orientations within individual layers resulting in multiple interfaces and an expanded design space.

In this study, carbon/epoxy pseudo-woven subassemblies are hybridized with traditional unidirectional layups to enhance impact and damage tolerance. Three different laminate configurations are assessed under high velocity impact according to ASTM D8101. During the experiments digital image correlation (DIC) and high-speed video were employed to evaluate the laminate's response. Preliminary results on 24 ply laminates indicate pseudo-woven architecture exhibits increased penetration resistance and reduced back face surface damage compared to traditional laminates.

Corresponding author: Subramani Sockalingam

1. INTRODUCTION

Traditional carbon fiber reinforced polymer matrix composite material systems play a critical role in various engineering applications. These composites exhibit brittle failure, limited toughness, and poor damage tolerance (stiffness-strength-toughness dilemma) [1]. These systems are often overbuilt, thus any increase in damage tolerance can yield significant cost and weight savings. Creating novel composite architectures aided by advanced manufacturing is an attractive approach to enhance toughness and damage tolerance in laminated composites. These composite systems

Copyright 2020. Used by the Society of the Advancement of Material and Process Engineering with permission.

used in aerospace structures need to be designed to withstand low and high velocity impact events [2].

3D woven laminates provide through thickness reinforcement and have been shown to prevent delamination, resist crack propagation, and increase toughness. 3D woven laminates are shown to have a stepwise fracture in tensile tests and a higher failure strain than their 2D counterparts. However, 3D woven laminate architecture reduces in-plane tensile strength and stiffness due to the reorientation of fibers [3]. Pseudo-woven (PW) laminates are proposed as an alternative laminate configuration to overcome the shortcomings of 2D and 3D laminates. PW laminates have been shown to have similar tensile properties while exhibiting enhanced damage tolerance compared to traditional composite configurations [3], [4], [5].

In this preliminary study, a woven-like composite laminate referred to as pseudo-woven was manufactured using unidirectional slit tapes. This laminate architecture uses an Automated Fiber Placement (AFP) technique to selectively alter the placement of tows in a layer resulting in a woven like architecture [3], [4], [5].

2. MANUFACTURING

2.1 Materials and curing

In this study three laminate configurations were manufactured using IM7 G/8552-1 slit tapes and were cured at 176 °C and 6.2 Bar. The first with PW laminates on the outer surfaces, referred to as Weave – Traditional – Weave or P1-WTW. The second with PW laminates on the inside called Traditional – Weave – Traditional or P2-TWT, and the third quasi-isotropic control traditional laminate called P3 - CONT. Each panel was manufactured using automated fiber placement with care taken to ensure proper tow alignment during layup, a critical aspect of PW manufacturing. These layup configurations will be discussed in section 2.4.

2.2 Pseudo-woven laminates

2.2.1 AFP Notation

PW laminates are manufactured through a manipulation of the layup process typically used in AFP manufacturing. Traditionally AFP manufacturing utilizes full tow coverage when laying tows placing full bands resulting in the conventional laminate construction. When manufacturing a PW laminate, tows are intentionally skipped to produce gaps in the bands. The gaps produced during skipping are filled in the subsequent passes compounding to produce the woven-like architecture. To understand the structure/architecture of the PW laminates, its manufacturing parameters and naming scheme are first discussed. The structure of a PW laminate is described using its AFP notation shown in Figure 1 [4], [5].

$$[\theta^1,\theta^2,\theta^3,\theta^4,..\theta^m]_a[x000x000]_{n\,b}[w]_c[ds]_d$$

Figure 1. A generic example of AFP notation (a) directional set (b) tow mask (c) physical tow width (d) directional shift [5]

AFP notation is broken down into four parts to describe the architecture of a PW laminate. Figure 1 (a) denotes fiber orientations used in the laminate, called the directional set. The directional set provides the orientations used in the laminate and the order in which orientations are laid. Using Figure 1 as an example, '$\theta^{1'}$ is laid, then '$\theta^{2'}$ to '$\theta^{m'}$, where 'm' is the number of fiber orientations in the laminate. The conventional definition of a ply is a layer of full coverage occupying a discrete Z position. Because of the apparent departure from conventional manufacturing for the PW laminates the authors have defined a ply as a completed directional set. The second grouping in Figure 1, subsection (b) represents the tow mask. This serves as a map of active, *x*, and inactive channels, *0*, of the AFP's head. The subscript *n* on the tow mask denotes the number of times the roller must pass over the domain to produce a panel of a specified width. For example, if a panel is sixteen tows wide then for this eight tow roller, n=2. The tow mask then is used to convey what channels are active and feed tows when the AFP's head makes its passes. Manipulation of this tow mask produces the woven-like architecture of the PW laminates. Figure 1 (c) represents the physical tow width, in this case 6.35 mm. It is possible for layups to have two adjacent active channels, where tow width is then defined as 12.7 mm.

Figure 1 (d) denotes directional shift, which takes effect after each directional set has been laid. Once a directional set has been laid, for a directional shift of *1*, the first fiber orientation in the previous directional set will shift to the end of the new set thus changing the directional set for the next ply. An example of directional shift is shown in Table 1, where column 'A' shows the effect of a directional shift of *1*, while column 'B' shows a shift of *0*. Note that the tow mask shifts irrespective of directional shift.

Table 1. An example of directional shift effect [5]

	A. Directional shift [1]		B. Directional shift [0]
A) Pass 1	$[\theta^1,\theta^2,\theta^3,\theta^4]$ [x000x000]n [6.35mm][1]	B) Pass 1	$[\theta^1,\theta^2,\theta^3,\theta^4]$ [x000x000]n [6.35mm][0]
A) Pass 2	$[\theta^2,\theta^3,\theta^4,\theta^1]$ [0x000x00]n [6.35mm][1]	B) Pass 2	$[\theta^1,\theta^2,\theta^3,\theta^4]$ [0x000x00]n [6.35mm][0]
A) Pass 3	$[\theta^3,\theta^4,\theta^1,\theta^2]$ [00x000x0]n [6.35mm][1]	B) Pass 3	$[\theta^1,\theta^2,\theta^3,\theta^4]$ [00x000x0]n [6.35mm][0]
A) Pass 4	$[\theta^4,\theta^3,\theta^2,\theta^1]$ [000x000x]n [6.35mm][1]	B) Pass 4	$[\theta^1,\theta^2,\theta^3,\theta^4]$ [000x000x]n [6.35mm][0]

Using the AFP notation, [45, 90,-45,0][x000x000]$_n$[6.35mm][0], the manufacturing of a PW panel used in the experiments is shown in Figure 2. In Figure 2 (a) the first directional set is laid onto the tool. The next pass, shown in Figure 2 (b) is laid in the same order as the previous set except the active channel shifts over one space. This process repeats in Figure 2 (c) and Figure 2 (d) completing the PW laminate sub-assembly.

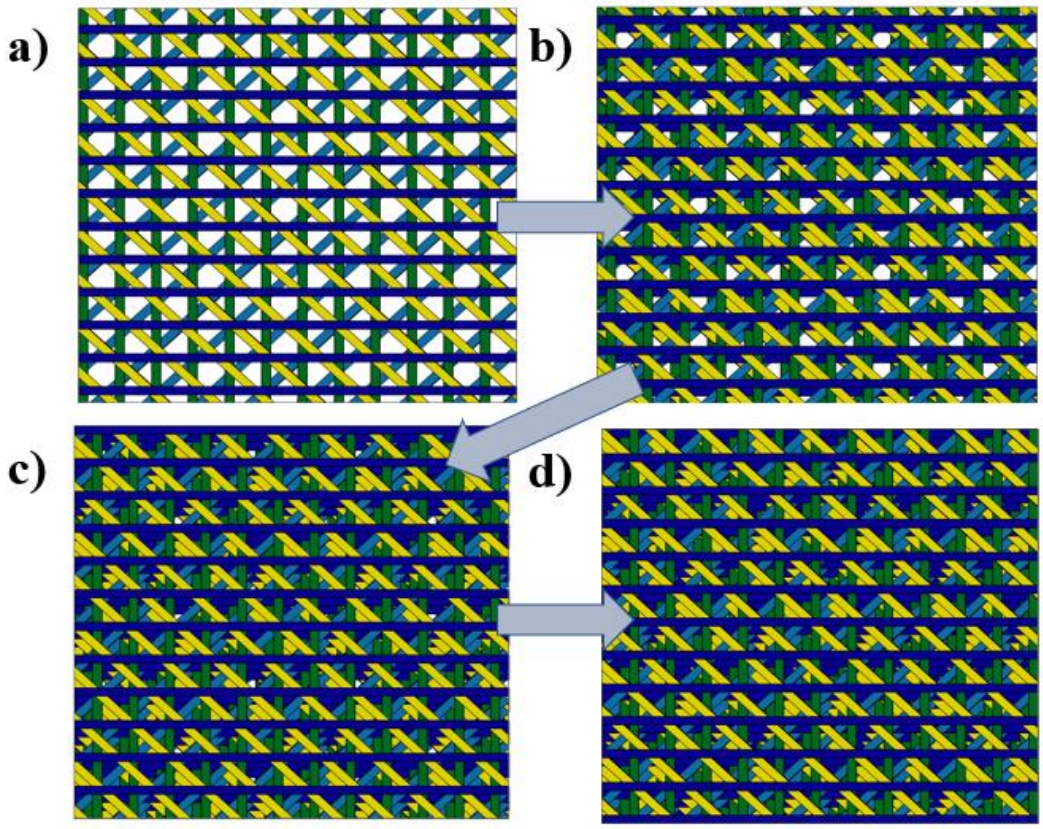


Figure 2. A depiction of the manufacturing process a) Pass 1 b) Pass 2 c) Pass 3 d) Pass 4

2.2.2 PW Naming Convention

The naming scheme for PW laminates directly represents their manufacturing parameters described in the AFP notation, for example: 4D-DS0-CS3 is a 4 ply laminate with 4 fiber orientations with adjacent active channels producing a double width tow represented here as *D*. The alternative to this would be a single width tow represented with an *S*. Directional shift is represented as *DS*, the number directly following *DS* is the quantity of the directional shift. The tow mask is represented by *CS* and is the number of inactive channels, or channels skipped, between active channels. The PW laminates manufactured for these experiments are 4S-DS0-CS3 and INV 4S-DS0-CS3. Their AFP notations are [45, 90, -45, 0][x000x000]n[6.35mm][0] and [0, -45, 90, 45][x000x000]n[6.35mm][0] respectively.

2.3 Hybridized panels

The manufacture of PW laminates is a time intensive process, PW laminates with 3 inactive channels between active channels take roughly four times longer to lay than a traditional laminate. As such, manufacturing an entirely PW laminate is an extremely time-consuming process. However, hybridizing a traditional laminate structure with PW laminates can be used to reduce manufacturing time while gaining attributes of PW laminates.

2.4 Laminate Manufacturing

For these experiments two hybrid structures are manufactured, the first configuration known as P1 - TWT is a panel with PW laminates sandwiched between traditional. Its stacking sequence is $[(45/90/-45/0)_2/4S\text{-}DS0\text{-}CS3/INV4S\text{-}DS0\text{-}CS3/(0/-45/90/45)_2]$. The other hybridized PW panel is a traditional laminate sandwiched between PW laminates, called P2 – WTW whose stacking sequence is $[4S\text{-}DS0\text{-}CS3_2/45/90/-45/0/0/-45/90/45/INV4S\text{-}DS0\text{-}CS3_2]$. The control sample's stacking sequence is a $[45/90/-45/0]_{3s}$ and is referred to as P3 - CONT. All panels manufactured for these tests are 24 plies thick. Panels made for this study were constructed using two different AFP machines, multiple panels of P1 - TWT, P2 - WTW, and P3 - CONT were made at the McNAIR Center University of South Carolina while one P2 - WTW panel was made at the NASA Langley Research Center. The University of South Carolina's AFP machine is a gantry machine with a refrigerated creel made by Ingersoll Machine Tools. The machine at the NASA Langley Research Center is made by Electroimpact, the machine is a robotic arm with an AFP head fixed to the end.

2.5 Specimen Preparation

Laminates were made into oversized sheets and trimmed to the 305mm (12 inch) by 305mm (12 inch) specimen specifications in ASTM Standard D8101 using a waterjet. After waterjet trimming edges were hand sanded to reduce the effect of boundary damage caused by cutting. A circular hole pattern was milled using a 4 flute carbide endmill on a CNC machine to ensure a proper fit on the test fixture. After specimens were trimmed and brought into geometrical specifications a coarse speckle pattern, Figure 3 was added onto the backside of the laminate. The speckle pattern was applied with spray paint using a stencil for each specimen.



Figure 3. A typical example of the speckle pattern used in experimentation.

3. EXPERIMENTATION

3.1.1 Experimental Setup

Impact tests were performed in accordance to the ASTM Standard D8101 at the NASA Glenn Research Center Ballistic Impact Lab. In this experiment, composite flat panels were impacted in the normal direction with hemispherical aluminum projectiles, Figure 4, weighing approximately 51 g. Specimens were clamped to the rear frame of the test fixture, Figure 5, by a circular frame with an inner diameter of 254.064 mm to ensure a rigid connection with the rear frame [6].

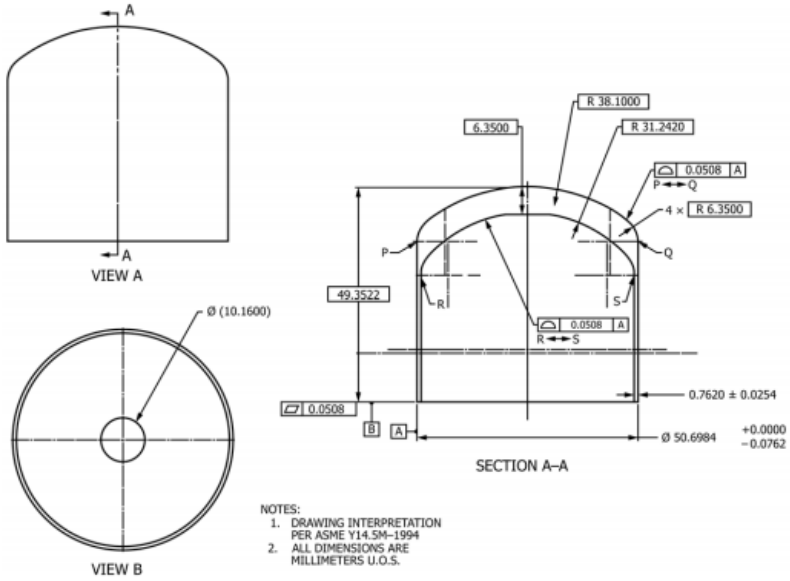


Figure 4. The technical drawing of the impactor used [6].

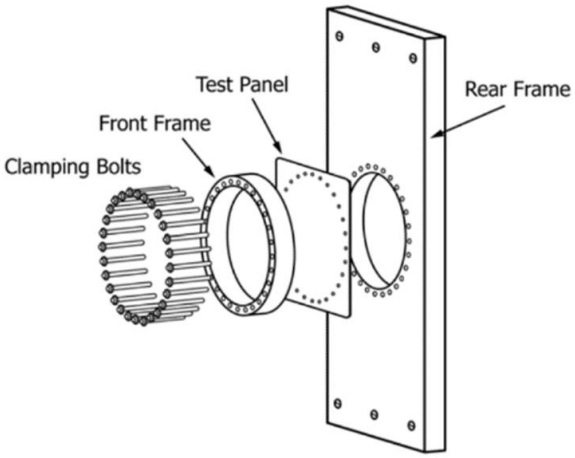


Figure 5. Exploded view of the test fixture [6].

Impactor velocities were determined using the TEMA motion analysis software by tracking a speckle pattern on the impactor. Multiple high-speed cameras were used to extract experimental

data with the assistance of ARAMIS and TEMA. The camera setup for experimentation is shown in Figure 6 multiple cameras are used to collect data from multiple viewpoints. A single camera on the side of the test housing was used to capture projectile's impact and rebound velocity. Another camera at the front of the impact housing, above the projectile barrel, was used to track the strike face. Camera pairs on the backside of the test housing were used to capture backside displacement using DIC. The DIC data was processed using ARAMIS.

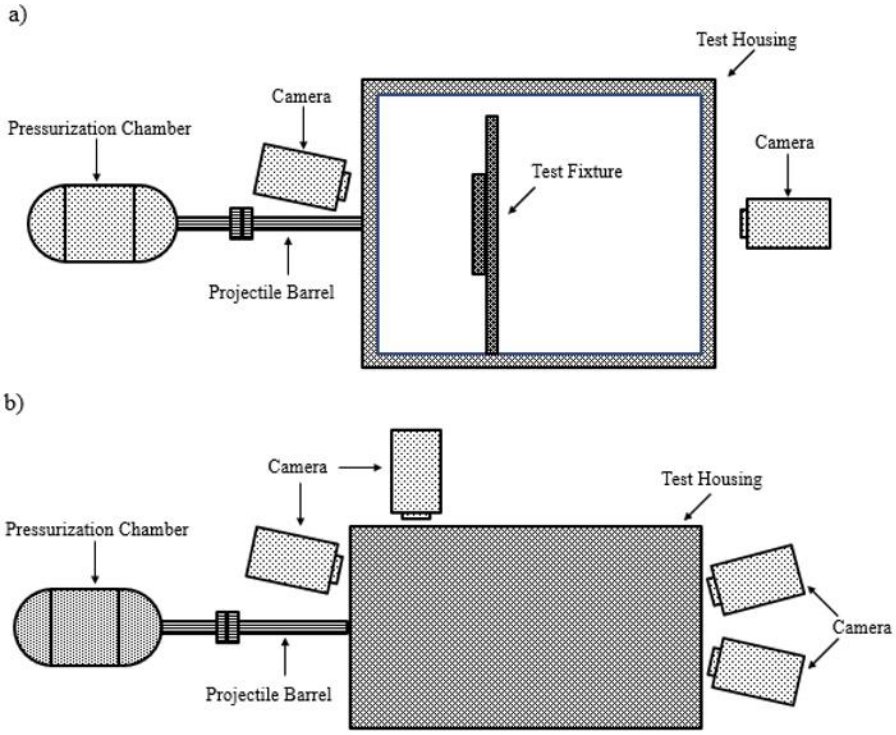


Figure 6. Multiple angles of the experimental camera setup. a) side view b) top view.

4. RESULTS AND DISCUSSION

4.1 Experimental Results

In this section, kinetic energy loss, $V_{50,}$ and displacement are used to assess the response of the laminate configurations. Due to the cost of the panels the sample size for the impacted specimens is relatively low. Five velocities were targeted for this series of tests, 76.20 m/sec (250 ft/sec), 91.44 m/sec (300 ft/sec), 106.68 m/sec (350 ft/sec), 114.30 m/sec (375 ft/sec), and 121.92 m/sec (400 ft/sec). Table 2 shows a summary of raw test results this data is used to tabulate results in the sections below.

Table 2. A table including the target impact velocities, test IDs, panel descriptions, projectile masses, impact velocities, rebound velocities, exit velocities, and results. 'Con' means that the projectile was contained while 'pen' means that the projectile penetrated the specimen. Where applicable U.S. customary units are shown in parenthesis.

Targeted Impact Velocity m/s (ft/s)	Test ID	Panel Description	Projectile Mass (g)	Impact Vel m/s (ft/s)	Rebound Vel m/s (ft/s)	Exit Vel m/s (ft/s)	Result
76.20 (250)	LVG1305	P1 - TWT	52.16	71.29 (233.9)	-30.67 (-100.65)	-	con
	LVG1301	P2 - WTW	51.89	78.05 (256.1)	-31.30 (-102.7)	-	con
	LVG1326	P3 - CONT	49.84	78.42 (257.3)	-33.23 (-109)	-	con
91.44 (300)	LVG1302	P1 - TWT	51.87	93.81 (307.8)	-40.78 (-133.8)	-	con
	LVG1297	P2 - WTW	52.03	89.15 (292.5)	-28.65 (-94.0)	-	con
	LVG1306	P3 - CONT	52.02	90.98 (298.5)	-35.14 (-115.3)	-	con
106.68 (350)	LVG1303	P1 - TWT	52.15	107.50 (352.7)	-34.77 (-114.1)	-	con
	LVG1298	P2 - WTW	51.99	109.48 (359.2)	-29.38 (-96.4)	-	con
	LVG1307	P3 - CONT	52.22	107.16 (351.6)	-33.30 (-109.27)	-	con
114.30 (375)	LVG1304	P1 - TWT	52.29	112.74 (369.9)	-37.49 (-123)	-	con
	LVG1300	P2 - WTW	51.94	112.07 (367.7)	-31.27 (-102.6)	-	con
	LVG1308	P3 - CONT	52.05	113.47 (372.3)	-	39.56 (129.81)	pen
121.92 (400)	LVG1327	P1 - TWT	50.33	120.67 (392.2)	-46.02 (-151)	-	con
	LVG1299	P2 - WTW	51.8	119.54 (395.9)	-	23.87 (78.34)	pen

4.1.1 V_{50}

The V_{50} for the different composite configurations is calculated with Equation 1. Where V_{RM} is the maximum impact velocity at which the laminate still rebounded the projectile. The variable V_P is the lowest velocity at which penetration occurred.

$$V_{50} = \frac{V_{RM} + V_P}{2} \quad [1]$$

Table 3 shows the computed V_{50} values, with P1 - TWT being greater than 120.67 m/s (392.2 ft/s) as the laminate did not penetrate at that impact velocity. V_{50} of P1 - TWT is around 8.5% higher than P3 - CONT and the V_{50} of P2 - WTW is 5.5% higher than P3 - CONT. This suggests that the incorporation of PW laminates increases the penetration resistance.

Table 3. Calculated V_{50} data

Laminate	V_{50} m/s (ft/s)
P1 – TWT	> 120.67 (392.20)
P2 - WTW	116.14 (381.05)
P3 - CONT	110.32 (361.95)

4.1.2 Kinetic energy loss

Residual kinetic energy was calculated as following ASTM standard D8101 with Equation 2. E_r is the residual kinetic energy and is computed from the projectile mass, M, and the residual velocity, V_r.

$$E_r = \frac{MV_r^2}{2} \quad [2]$$

Impact Kinetic energy was calculated using Equation 3 from ASTM standard D8101. Impact kinetic energy, E_i, is computed from the projectile mass, M, and the projectile impact velocity, V_i.

$$E_i = \frac{MV_i^2}{2} \quad [3]$$

Kinetic energy loss was calculated as demonstrated in ASTM standard D8101 with Equation 4 where loss in kinetic energy of the projectile as a result of impact is computed.

$$E_a = E_i - E_r \quad [4]$$

Specimens were impacted at 5 different velocities resulting in clusters around the 150 J, 220 J, 300 J, 330 J, and 360 J impact kinetic energy levels, test data is plotted in Figure 7. The first cluster at 150 J shows that P2 - WTW had the most kinetic energy loss while P1 - TWT had the least. The 220 J cluster has all configurations showing similar results with the P3 - CONT being marginally lower than the rest. The 300 J cluster shows almost indistinguishable differences between the P1 - TWT and P3 - CONT configurations while the P2 - WTW has the highest loss. At the 330 J cluster all configurations seem to be nearly equal with the P2 - WTW configuration being marginally higher than the rest. It is important to note that the P3 - CONT configuration exhibits complete penetration at this impact energy. In the 375 J group P1 - TWT has the lowest loss in impactor kinetic energy while the P2 - WTW configuration has a higher loss and exhibits penetration. The PW hybrid laminates see higher energy absorption than their conventional counterpart in both configurations at every impact energy.

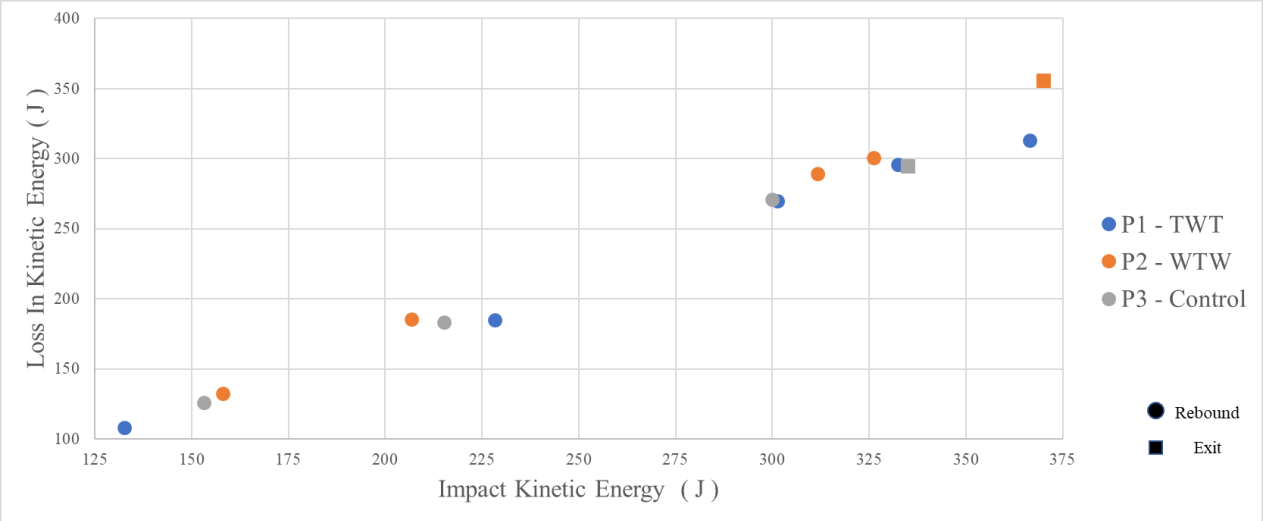


Figure 7. Residual Kinetic Energy vs Impact Kinetic Energy. Circular data points represent non-penetrating or rebounded impactors. Square data points represent penetrating or exiting impactors.

4.1.3 Displacement

Back face displacement was determined using the DIC data taken from the ARAMIS software. The DIC software mapped displacement data into the contours seen in Figure 8. The contours selected for this figure are at 3 different impact velocities, 106.68 m/s (350 ft/sec), 114.30 m/s (375 ft/sec), and 121.92 m/s (400 ft/sec). The images shown in Figure 8 represent peak displacement in the impact event. Peak displacement was determined using a plot output in ARAMIS seen in Figure 9 where Points are placed along a line drawn through the center of the specimen seen in Figure 8. When all points show peak displacement, as shown by the red x's in Figure 9 the corresponding video frame is extracted and is used as peak. Discontinuities in the displacement data are due to the paint breaking from the backside of the specimen during the impact event. Because of the nature of impact some of the contours have an artificially high displacement due to specimen and paint breakage. This value does not represent the behavior of the laminate but rather a small failed portion.

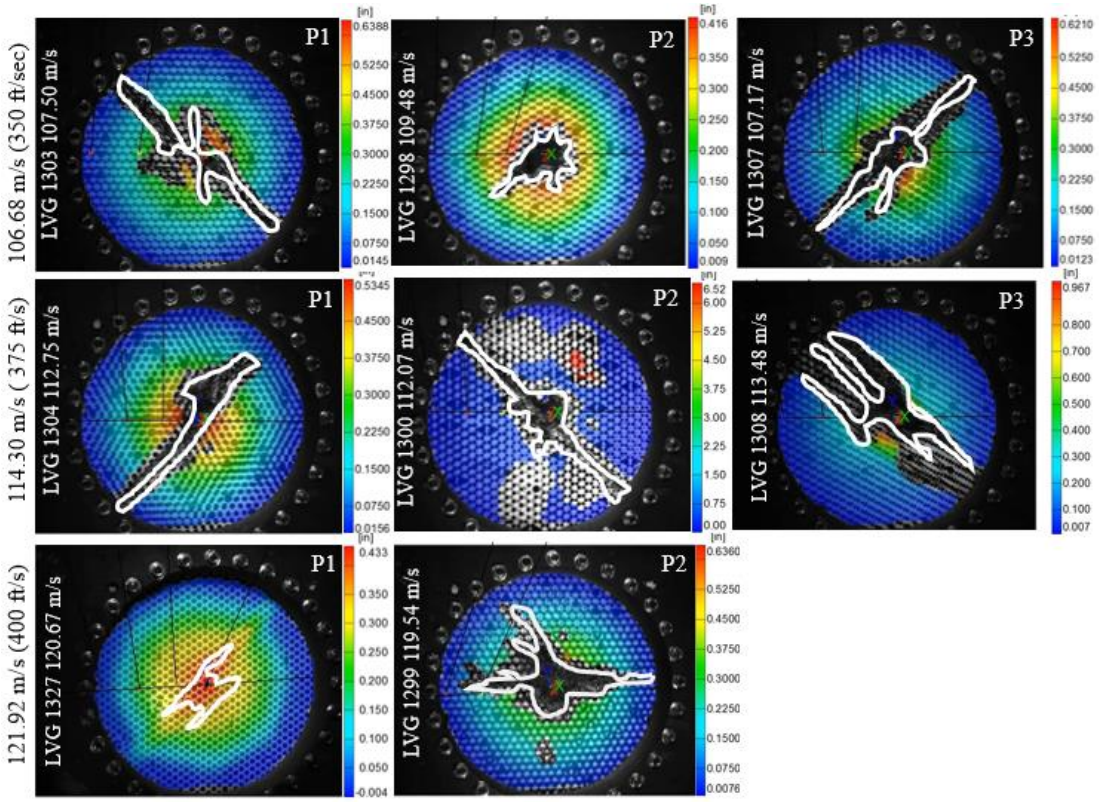


Figure 8. DIC contours and outlined backside surface damage for three different target impact velocities. Displacement contour units are in inches.

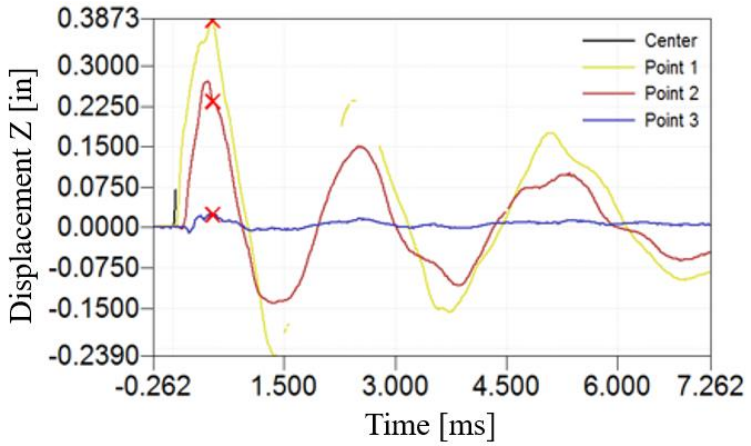


Figure 9. The points used to map displacement and detect peak displacement, shown by red x's, for test LVG 1297

The displacement along the cross-sectional area of specimens at peak displacement at the 91.44 m/s (300 ft/sec) impact velocity are given in Figure 10. Displacement data was taken from the black line bisecting the specimens seen in Figure 8 this is referred to as section 0. This impact velocity serves as a representative example of the entire sample set which all follow the same trend. Displacement along the section 0 at peak displacement shows P3 - CONT with the highest displacement while P1 - TWT has the lowest. All specimens show a gap where displacement data was lost due to the impactor breaking the speckle pattern from the backside of the specimen. The experimental data suggests that the back face deflection of PW hybridized configurations are lower than their conventional counterpart.

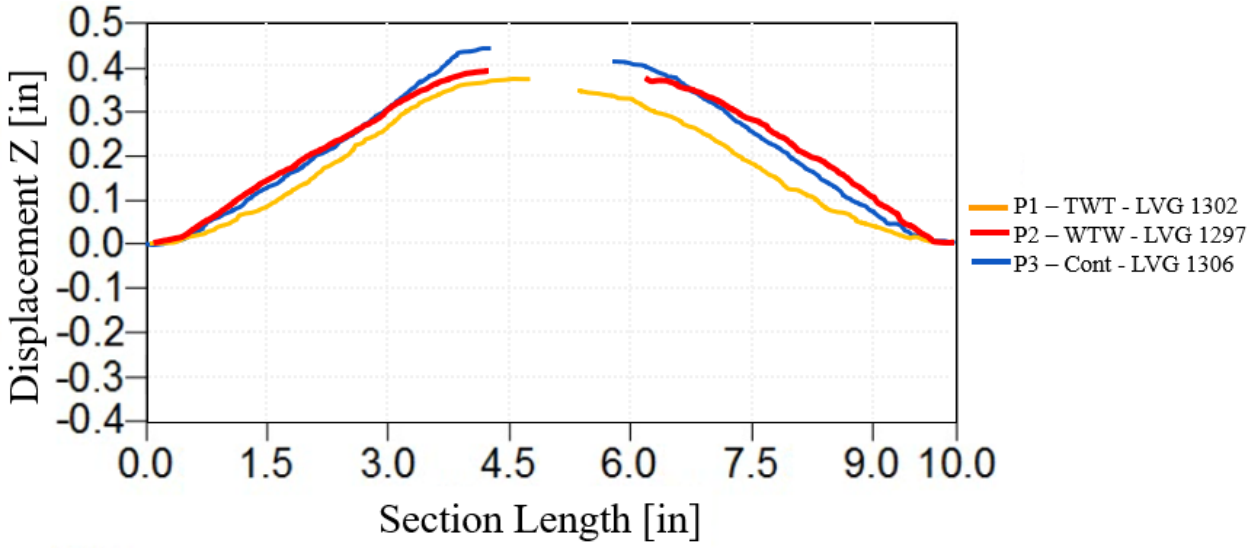


Figure 10. A superimposed image of displacement along the section 0 taken from the 91.44 m/s (300 ft/sec) impact velocity. The orange, red, and blue lines represent P1 – TWT, P2 – WTW, and P3 – CONT respectively.

4.1.4 Damage footprint

Superimposed onto the displacement contours given in Figure 8 is a white outline indicating the surface damage on the back face of the specimen. The hybridized PW laminates sustain a smaller damaged surface area at each impact velocity. There is not an P3 - CONT impact test for the 121.91 m/s (400 ft/s) due to penetration occurring at the 114.30 m/s (375 ft/s) impact velocity. It is interesting to note that both the P1 - TWT and P2 - WTW configurations demonstrate smaller surface area damage than the traditional configuration.

5. CONCLUSION

Three 24 ply carbon/epoxy hybrid pseudo-woven laminate configurations are manufactured in this study using AFP. One with semi-woven laminate on the inside (named as P1-TWT), second with semi-woven laminate on the outer surfaces (named as P2-WTW) and third quasi-isotropic control laminate $[45/90/-45/0]_{3s}$ named as P3-CONT. High velocity impact tests are conducted according to the ASTM D8101 standard. The hybridized configuration P1-TWT where the PW laminates are on the inside showed the highest penetration resistance V50, 8.5% greater than the control. The experimental results also indicate reduced back face damage and back face deflection for the hybridized laminates compared to the control layups. Further investigation using nondestructive evaluation is required to better understand the damage within the laminates.

6. ACKNOWLEDGEMENTS

The authors would like to thank Dr. Michael Pereira of NASA Glenn Research Center for the high velocity impact testing support, Dr. Dawn Jegley and the ISAAC team at NASA Langley Research Center for their contributions towards manufacturing one of the pseudo-woven panels. The authors CVR and SS gratefully acknowledge financial support from the SC Space Grant Consortium. The authors would also like to acknowledge the University of South Carolina's McNAIR Center for their support in AFP manufacturing.

7. REFERENCES

[1]. Czél, G., Jalalvand, M., Wisnom, MR. "Demonstration of pseudo-ductility in unidirectional hybrid composites made of discontinuous carbon/epoxy and continuous glass/epoxy plies." *Composites Part A* (2015). 75- 84.10.1016/j.compositesa.2015.01.019

[2]. Cantwell, W. J., Morton, J. "The impact resistance of composite materials---a review." *Composites* 1991: 347- 362. doi:10.1016/0010-4361(91)90549-V

[3]. Nagelsmit, M., Kassapoglou, C., Gurdal, Z. "A New Fibre Placement Architecture for Improved Damage Tolerance" (2010).

[4]. Vakili Rad, C., Thomas, F., Sockalingam, S., Gurdal, Z. "Low Velocity impact response of hybrid pseudo-woven fiber-reinforced composite laminates" SAMPE Conference (2019)

[5]. Vakili Rad, C., Thomas, F., Seay, B., Van Tooren, M., Sockalingam, S. "Manufacturing and characterization of novel clutch non-conventional fiber-reinforced composite laminates." *Composite Structures* (2019). 10.1016/j.compstruct.2019.02.018.

[6]. ASTM Standard D8101/D8101M-17, 2017. "Stand Test Method for Measuring the Resistance of Composite Materials to Impact by a Blunt Projectile" ASTM International, West Conshohocken, PA, 2017 DOI: 10.1520/D8101_D8101M-17, www.astm.org